

Mode Structure of Locked-Mode-Like Instability in LHD and Its Effects on Confinement Degradation

Yuki TAKEMURA^{1,2)}, Ryo YASUHARA^{1,2)}, Hisamichi FUNABA¹⁾, Hiyori UEHARA^{1,2)},
D. J. Den HARTOG³⁾, Kiyomasa WATANABE^{1,4)}, Satoru SAKAKIBARA^{1,2)},
Yoshiro NARUSHIMA^{1,2)} and Satoshi OHDACHI^{1,5)}

¹⁾National Institute for Fusion Science, National Institutes of Natural Science, Toki, Gifu 509-5292, Japan

²⁾The Graduate University for Advanced Studies, SOKENDAI, Toki, Gifu 509-5292, Japan

³⁾University of Wisconsin-Madison, Department of Physics, Madison, Wisconsin, USA

⁴⁾Nagoya University, Graduate School of Engineering, Chikusa, Nagoya 464-8603, Japan

⁵⁾The University of Tokyo, Graduate School of Frontier Sciences, Kashiwa, Chiba 277-8561, Japan

(Received 20 April 2021 / Accepted 24 June 2021)

The internal mode structure of a precursor with the tearing-parity structure of the locked-mode-like instability is investigated. For the first time, the Thomson scattering system with high temporal and spatial resolution enables us to find the non-rotating temperature flattening region in the torus outboard side in addition to the rotating island during the slowing-down phase. Additionally, the width of the flattening region is 10% normalized by the plasma minor radius. Furthermore, the radial profiles of the pressure degradation during the slowing-down phase are evaluated. At the beginning of the slowing-down phase, the pressure degradation area is located slightly inside the resonant surface. After that, the peak location moves to the core region. Finally, the degradation area peaks at the plasma center.

© 2021 The Japan Society of Plasma Science and Nuclear Fusion Research

Keywords: locked mode, magnetic island, ideal interchange mode, MHD instability, LHD

DOI: 10.1585/pfr.16.1402091

1. Introduction

The locked-mode-like instability related to the plasma collapse appears when the plasma current increasing the rotational transform increases in the low magnetic shear configuration of the Large Helical Device (LHD) [1–3]. In such discharges, the ideal interchange mode is considerably unstable [4]. The locked-mode-like instabilities are categorized into two types depending on the internal mode structure of the precursor [5]. An interchange-type precursor has a radial displacement profile similar to the interchange mode. On the other hand, a tearing-type precursor has a profile similar to the tearing mode [6, 7]. For both instabilities, the precursor frequency decreases to zero; furthermore, when its frequency is almost zero, the non-rotating mode rapidly grows, and the core pressure gradient rapidly decreases. It should be noted that the onset regimes of the two instabilities in the diagram of the beta value and the magnetic shear are different [5].

In previous works, the physical mechanism of the slowing-down related to the plasma collapse in the locked-mode-like instability has been investigated. In the discharges with the error field, it was found that the slowing-down occurs due to the $\mathbf{j} \times \mathbf{B}$ torque caused by the interaction between the external static resonant magnetic perturbation (RMP) and the perturbed current induced by the pre-

cursor of either instabilities [8]. On the other hand, the internal mode structure of the precursor during the slowing-down phase has also been investigated. The qualitative difference in the mode structure of the interchange-type precursor and the tearing-type precursor was observed via the electron cyclotron emission measurement, the soft X-ray measurement, and the CO₂ laser interferometry [1, 6].

In the LHD, the fine electron pressure profile can be obtained using the Thomson scattering (TS) system with high spatial resolution (~ 0.02 m along the major radius) [9]. This diagnostic is called the conventional TS system. Therefore, the narrow pressure flattening around the resonant surface has been successfully observed. On the other hand, it is difficult to evaluate the radial profile of the pressure fluctuation due to the MHD instability because the frequency of the fluctuation often exceeds several hundred Hz. The frequency is much higher than that of the conventional TS system (~ 33 Hz). However, a high-repetition-rate Nd:YAG laser has been recently installed in the LHD for the new TS system (which is referred to as the fast TS system). This fast TS system enables us to obtain the rapid change of the electron temperature profile with high spatial resolution and evaluate the radial profile of the electron temperature fluctuation due to the precursor.

In this work, the electron temperature fluctuations due to the tearing-type precursor of the locked-mode-like in-

author's e-mail: takemura.yuki@nifs.ac.jp

stability were obtained using the fast TS system with a short time interval of 1 kHz, and the fine mode structures in the middle part and last part of the slowing-down phase were evaluated. In addition, the effects of the precursor and the rapid growth of the non-rotating island on the time-averaged pressure profile were also investigated.

2. Experimental Setup

In the LHD configuration, the core rotational transform increases, and the magnetic shear decreases with the increase of the aspect ratio, A_p [10]. In order to obtain the low-shear plasmas, A_p was set to 7.6, which is higher than the value of the standard configuration (5.8). As the error field affects the behavior of the precursor [8], the error field is almost canceled upon application of the external RMP using the external supplement coils [11].

The frequency, amplitude and poloidal/toroidal mode number (m/n) of the magnetic fluctuation due to the precursor of the locked-mode-like instability were measured using magnetic probe arrays [12]. The amplitude of the magnetic fluctuation with almost zero frequency was measured via saddle loop arrays. The time-averaged pressure profile was evaluated using the conventional TS system. The radial profile of the electron temperature fluctuation due to the precursor was evaluated through the fast TS system. It should be noted that the measurement time of the fast TS system with an interval of 1 kHz was limited to 30 ms. By contrast, the conventional TS system with an interval of 33 Hz can measure the pressure profile until the plasma terminates. As the conventional TS system and the fast TS system have a common detector and different probe lasers, both systems can measure the electron temperature in the same discharge by adjusting the trigger time of the probe lasers.

Figure 1 shows the discharge waveforms of the locked-mode-like instability with the tearing-type precursor, where the internal mode structure during the slowing-down phase can be measured via the fast TS. Figures 1 (a)–(g) show the time evolution of the volume-averaged beta, the line-averaged electron density, the plasma current normalized by the operational magnetic field strength, the poloidal magnetic fluctuation with $m/n = 1/1$, its frequency, the amplitude of the $m = 1$ non-rotating radial magnetic fluctuation, and the resonant surface location estimated from the center of the flattening region of the electron temperature profile, respectively. The neutral beams (NBs) for the plasma production and heating are injected in the time range from $t = 3.3$ to 4.7 s. The plasma current increasing the rotational transform is driven by the NBs, and the current value gradually increases to ~ 20 kA/T. In the #160553 discharge (the black solid line in Fig. 1), the $m/n = 1/1$ mode with a frequency of ~ 1.4 kHz appears at $t = 3.7$ s as the precursor. The frequency of the precursor starts to decrease at 3.82 s after the constant rotating phase, where the frequency and the magnetic fluctuation ampli-

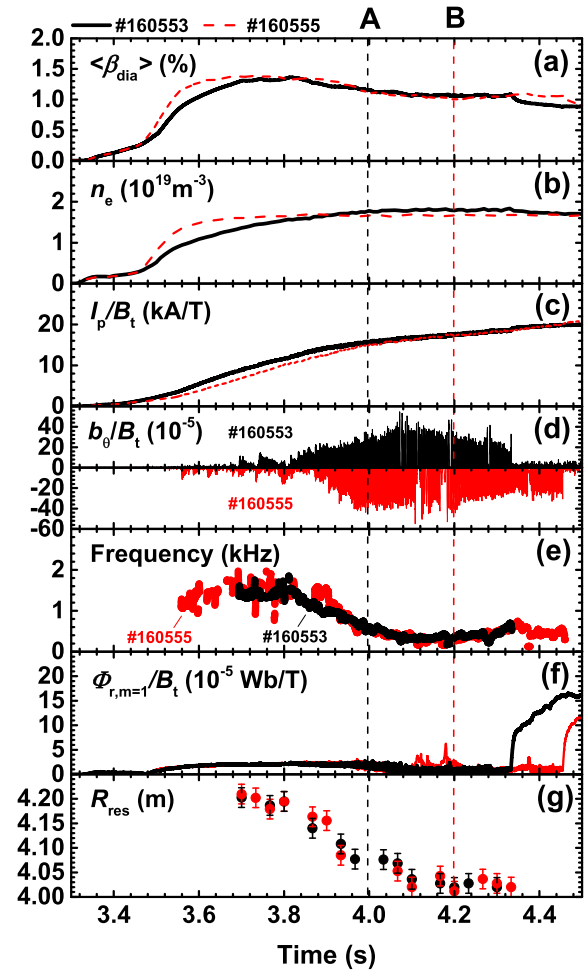


Fig. 1 Waveforms of the discharges of the locked-mode-like instability with the tearing-type precursor. (a) Volume-averaged beta value, (b) line-averaged electron density, (c) plasma current normalized by the operational magnetic field strength, B_t , (a positive current leads to an increase in the rotational transform), (d) poloidal magnetic fluctuation with $m/n = 1/1$, (e) frequency of a peak wavelet component of its fluctuation, (f) amplitude of the non-rotating radial magnetic fluctuation evaluated via saddle loop arrays, and (g) resonant surface location. The vertical dashed lines marked with the letters A and B correspond to the measurement times of the fast TS system in the #160553 discharge (black lines) and #160555 discharge (red lines), respectively.

tude are almost constant. Here, the slowing-down phase continues from $t = 3.82$ to 4.33 s. In the slowing-down phase, the frequency decreases, the magnetic fluctuation amplitude increases, and the volume-averaged beta value gradually decreases. According to a previous work [5], the slowing-down phase is categorized into two stages depending on the process through which the plasma flow on the resonant surface decreases. In the first stage of the slowing-down phase, the resonant surface moves to the core region, where the plasma flow is small. In the second stage, the plasma flow itself decreases even if the res-

onant surface does not move significantly. As shown in Fig. 1 (g), the time region from 3.82 to 4.1 s, during which the resonant surface at 4.2 m moves to 4.0 m, and the time region from 4.1 to 4.33 s, during which the resonant surface is almost constant, are considered to be the first and second stage, respectively.

At $t = 4.33$ s, the precursor rotation stops, and the amplitude of the radial magnetic fluctuation with $m/n = 1/1$ rapidly increases, resulting in a further reduction in the volume-averaged beta value. By contrast, the red lines show the waveforms of another discharge (#160555), during which the electron temperature profile is also measured via the fast TS system. It should be noted that both discharges exhibit a similar waveform behavior of the time evolution except for the timing of the rapid growth of the non-rotating magnetic fluctuation.

3. Experimental Results

Figure 2 shows the radial mode structure of the precursor measured via the fast TS system at $t = 4.0$ s in the slowing-down phase in the #160553 discharge (denoted as time A in Fig. 1). It should be noticed that $t = 4.0$ s corresponds to the last part of the first stage in the slowing-down phase, which means that the resonant surface moves to the low-flow region. Here, the amplitude and the phase difference of the electron temperature fluctuations are evaluated based on the conditional average technique [13] using the magnetic probe signal. Here, the amplitude and the phase difference of the electron temperature fluctuations are evaluated based on the conditional average technique [13] using the magnetic probe signal. The reason for applying the conditional average technique is that the sampling time of the fast TS system signals is too long (1 ms) for a precursor frequency of about 500 Hz.

Figures 2 (a)-(d) show the radial profile of the time-averaged electron temperature during the oscillation of the precursor, the coefficient of determination, R^2 , when the conditional averaged data is fitted by a trigonometric function, the electron temperature fluctuation amplitude normalized by the time-averaged electron temperature of Fig. 2 (a), and the phase difference between the magnetic fluctuation and the electron temperature fluctuations, respectively. Here, it is assumed that the amplitude and the phase difference with $R^2 > 0.2$ are meaningful. On the horizontal axis, r_{eff} corresponds to the minor radius of a circular cross section equivalent to the plasma poloidal cross section. The positive/negative sign denotes the torus outboard/inboard side. The mapping between r_{eff} and the major radius of the TS system sight line was performed using the equilibrium data such that the time-averaged electron temperatures in the torus outboard and inboard sides are consistent with each other. The profile of the electron temperature fluctuation amplitude in Fig. 2 (c) has two peaks at $r_{\text{eff}} \approx 0.3$ m, and the phases of these peaks are inverted, as shown in Fig. 2 (d). This suggests that the precursor has

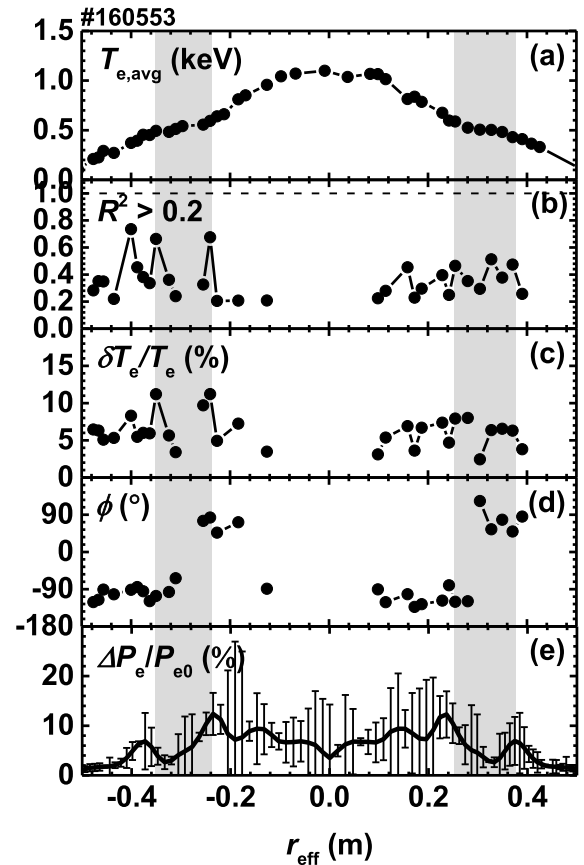


Fig. 2 Radial profiles of the electron temperature signals measured using the fast TS system at $t = 4.0$ s (time A of Fig. 1). (a) Time-averaged electron temperature, (b) coefficient of determination between the conditional average of the electron temperature fluctuations due to the precursor and its fitting function, (c) electron temperature fluctuation amplitude, (d) phase difference between the magnetic fluctuation and the electron temperature fluctuations, and (e) pressure degradation level from $t = 3.97$ to 4.07 s. In panels (b)-(d), only the data for channels with coherence > 0.7 are displayed. The hatched area corresponds to the rotating magnetic island region.

the tearing-parity structure. The rotating magnetic island is supposed to be located between these peaks, as shown in the hatched area of Fig. 2. The island width, which was evaluated from the interval between the two peaks, is $W \approx 0.12$ m ($W/a_p \approx 25\%$) for both the torus inboard and outboard sides. Here, a_p is the plasma minor radius. The center of the island is $r_{\text{center}} \approx 0.3$ m ($r_{\text{center}}/a_p \approx 0.6$). In order to investigate the effect of the precursor on the time-averaged pressure profile, Fig. 2 (e) shows the profile of the time-averaged electron pressure degradation during an interval of 0.1 s from $t = 3.97$ to 4.07 s measured via the conventional TS system. This profile was normalized by the central electron pressure. It should be noted that the pressure is time-averaged during an interval of 0.17 s (five sequential time slices) in order to remove the effect of the perturbed pressure due to the precursor. This average

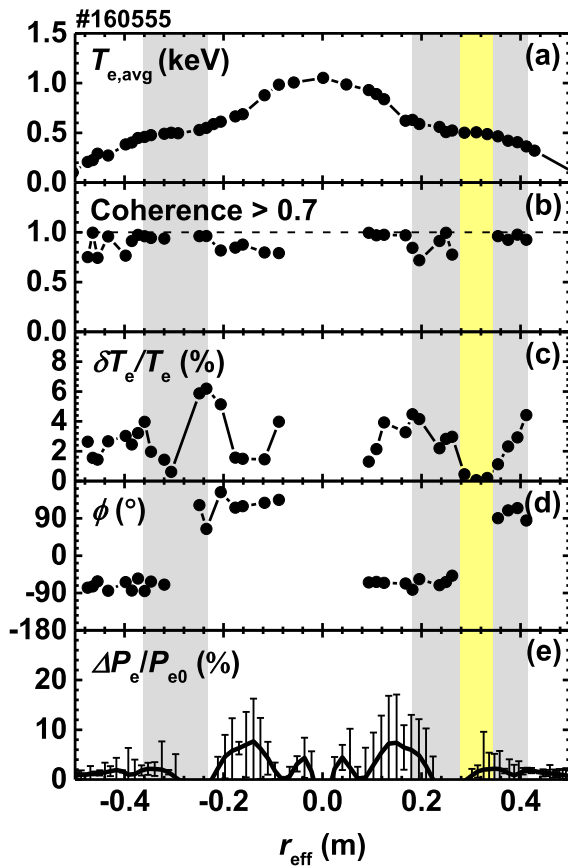


Fig. 3 Radial profiles of the electron temperature signals measured using the fast TS system at $t = 4.2$ s (time B of Fig. 1). (a) Time-averaged electron temperature, (b) coherence between the magnetic fluctuation and the electron temperature fluctuations due to the precursor, (c) electron temperature fluctuation amplitude, (d) phase difference between the magnetic fluctuation and the electron temperature fluctuations, and (e) pressure degradation level from $t = 4.17$ to 4.27 s. Only the data for channels with coherence > 0.7 is displayed in panels (b) and (d), whereas the data for channels with coherence > 0.7 or $\delta T_e \approx 0$ are displayed in panel (c). The grey hatched area corresponds to the rotating magnetic island region. The yellow hatched area corresponds to the non-rotating flattening region.

method was also applied to the pressure profile shown in Figs. 3 and 4. The error bar is mainly due to the scattering of the electron density profile measured via the conventional TS system. The pressure degradation region is located in the area ranging from the center of the island to the plasma center, and its level is almost constant. This result suggests that the pressure profile around the magnetic island is flattened, and the pressure in the core region is also reduced.

Figure 3 shows the radial mode structure of the precursor measured via the fast TS system at $t = 4.2$ s in the slowing-down phase in the #160555 discharge (denoted as time B in Fig. 1). It should be noticed that $t = 4.2$ s corresponds to the middle part of the second stage during the

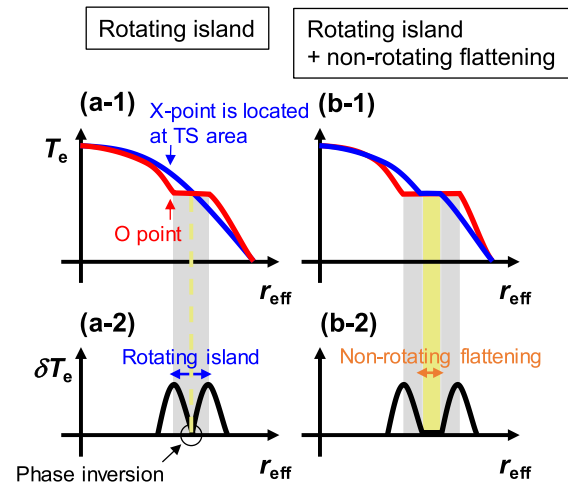


Fig. 4 Conceptual diagrams of the radial profiles of (a-1) and (b-1) the electron temperature when the O/X-point of the rotating island is located on the TS system sight line and (a-2) and (b-2) the amplitude of the electron temperature fluctuation due to the rotating island. Panels (a-1) and (a-2) show the rotating island, whereas panels (b-1) and (b-2) show the non-rotating flattening in addition to the rotating island. The δT_e profiles shown in panels (a-2) and (b-2) are similar to those presented in Fig. 2 and Fig. 3, respectively. The grey hatched area corresponds to the rotating magnetic island region, and the yellow hatched area corresponds to the non-rotating flattening region.

slowing-down phase [8], which means that the resonant surface does not move significantly, and the plasma flow itself slows down. The data in Fig. 3 does not belong to the same discharge as that illustrated in Fig. 2. However, the behavior of the beta value, the line-averaged electron density, the plasma current, the magnetic fluctuation amplitude, and the mode frequency are almost the same as those of Fig. 2 except for the timing of the rapid growth of the non-rotating magnetic fluctuation, which was discussed in Sec. 2. Figures 3(c) and (d) show that, even in the second stage, the precursor has the tearing-parity structure. Here, the amplitude and the phase difference were evaluated using the fast Fourier transform analysis because the fluctuation frequency (~ 250 Hz) is sufficient low. The peak value of the electron temperature fluctuation amplitude is not changed significantly compared with that in the first stage. On the other hand, the magnetic island width is ~ 0.23 m ($W/a_p \approx 50\%$) for $r_{\text{eff}} > 0$ and ~ 0.12 m ($W/a_p \approx 25\%$) for $r_{\text{eff}} < 0$. Compared with the first stage, the island width is not changed significantly for $r_{\text{eff}} < 0$, but the width doubles for $r_{\text{eff}} > 0$, which means that the width for $r_{\text{eff}} > 0$ is larger than that for $r_{\text{eff}} < 0$. It should be noted that, for $r_{\text{eff}} > 0$, there is the region where the fluctuation amplitude is almost zero, as shown in the yellow hatched area of Fig. 3, and the width of the region is ~ 0.05 m (10% normalized by a_p), whereas the width is not clear for $r_{\text{eff}} < 0$. The reason for the different island

widths in the torus outboard and inboard sides is discussed in the next section. The center of the rotating island is $r_{\text{center}}/a_p \approx 0.6$, which is almost the same as that in the first stage. The poloidal magnetic fluctuation amplitude measured outside the plasma in the second stage is $\sim 30 \times 10^{-5}$, which is larger than that in the first stage ($\sim 20 \times 10^{-5}$). In addition, Fig. 3 (e) shows the effect of the precursor on the time-averaged pressure profile in the second stage, which suggests that the pressure degradation level is reduced in the core region, and the degradation region is located from $r_{\text{eff}} \approx 0.1$ to ≈ 0.25 m.

4. Discussion and Summary

Figure 4 shows the conceptual diagrams of the relationship between the electron temperature profile and the profile of the electron temperature fluctuation amplitude (δT_e) when the island rotates. Here, T_e is assumed to be constant in both space and time in the island region. When the X-point of the island is located on the TS system sight line, there is no flattening in the electron temperature profile, as shown in Fig. 4 (a-1). However, when the O-point is located on the sight line, the flattening region exhibits the maximum width. In this situation, δT_e at the phase-inversion location is zero (Fig. 4 (a-2)), which means that the electron temperature at the phase-inversion location is constant during the island rotation. On the other hand, when the non-rotating flattening occurs in addition to the rotating island, the flattening region of the temperature profile is always observed regardless of the O/X-point of the rotating island, as shown in the yellow hatched area of Fig. 4 (b-1). In this situation, a region with a finite width appears, where δT_e is almost zero.

According to the radial mode structure of the precursor at the middle part of the second stage during the slowing-down phase, the finite width region with $\delta T_e \approx 0$ is observed around the resonant surface for $r_{\text{eff}} > 0$, as shown by the yellow hatched area of Fig. 3. This indicates that the electron temperature is constant in this region during the island rotation. Moreover, the time-averaged electron temperature profile is flat, as shown in Fig. 3 (a). These results suggest that the non-rotating flattening occurs.

There are several possible interpretations for the observation that the non-rotating flattening is located at the torus outboard side: (1) The stochasticization of the magnetic flux at the X-point of the rotating island radially expands when the X-point is located at the torus outboard side. (2) The non-rotating component of the radial magnetic field with $m/n = 1/1$ appears in addition to the rotating component. (3) The asymmetric perturbed pressure profile is caused by the non-rotating ballooning instability. For interpretation (2), the non-rotating component of the radial magnetic field with $m/n = 1/1$ is not clearly observed during the slowing-down phase using the presently installed saddle loops. This is due to the following reason.

The width of the non-rotating flattening region is 0.05 m ($W/a_p \approx 10\%$). Assuming there is an island with a width of 10% , its width is converted into the magnetic fluctuation amplitude measured via the saddle loop arrays displayed in Fig. 1 (f); this corresponds to the small amplitude of $\sim 3 \times 10^{-5}$ Wb/T. Therefore, it is difficult to detect this non-rotating component of the radial magnetic field with $m/n = 1/1$ using the magnetic diagnostics. In order to clarify the mechanism for the non-rotating flattening, an investigation of the stochasticization in the torus outboard/inboard sides and the ballooning instability is required through numerical simulations based on the experimental conditions. These are the future subjects.

Figure 5 shows the time evolution of the pressure degradation profile during the slowing-down in the #160553 discharge of Fig. 1: panel (a) shows the profile at the beginning of the first stage of the slowing-down phase; panel (b) shows the profile at the last part of the first stage, which is the same as time A of Fig. 1; panel (c) shows the profile at the beginning of the second stage; panel (d) shows the profile at the middle part of the second stage,

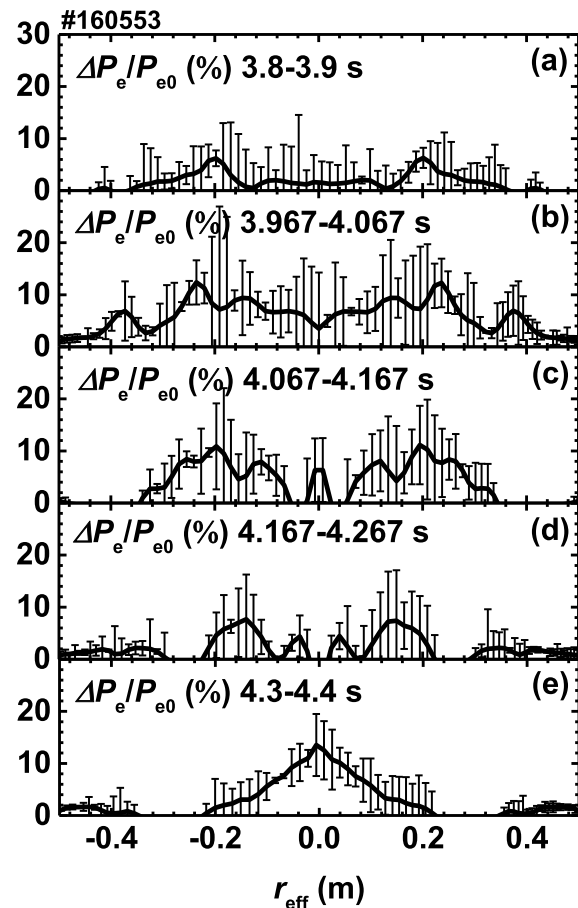


Fig. 5 Radial profiles of the electron pressure degradation level between (a) $t = 3.8$ and 3.9 s, (b) $t = 3.967$ and 4.067 s, (c) $t = 4.067$ and 4.167 s, (d) $t = 4.167$ and 4.267 s, and (e) $t = 4.3$ and 4.4 s. The degradation level is normalized by the central pressure. The time interval is 0.1 s.

which is the same as time B of Fig. 1; and panel (e) shows the profile before and after mode-locking. In each case, the time interval is 0.1 s. The degradation level of the stored energy at each time is 8%, 7%, 4%, 0%, and 13%, respectively. Starting from 4.33 s, the non-rotating island rapidly grows, and the phase of the O-point of the non-rotating island is 30° at the poloidal cross section, which is the measurement location of the TS system. Here, the phase increases counterclockwise from $Z = 0$ on the outboard side, and the line of sight of the TS system is located at $Z = 0$ on the outboard/inboard sides. At the beginning of the first stage, the pressure degradation area appears to be located slightly inside the resonant surface with $r_{\text{eff}} \approx 0.3$ m. However, in the last part of the first stage, the degradation region expands from the $m/n = 1/1$ resonant surface to the plasma center, and its level almost doubles. Furthermore, from the beginning part of the second stage to the middle part, the degradation profile in the core region decreases, the peak location moves to the core region, and the peak value gradually decreases. Finally, the degradation level peaks at $r_{\text{eff}} \approx 0$ m. By contrast, the rotating island width at the torus outboard side normalized by a_p is 25% at 4.0 s and 50% at 4.2 s, as shown in Figs. 2 and 3. These results suggest that the peak value of the pressure degradation level does not depend on the rotating island width, but the degradation region is related to the island width.

In this study, the internal mode structure of the tearing-type precursor of the locked-mode-like instability was measured using the fast TS system with high spatial and temporal resolution. It was found that, in the first stage of the slowing-down phase, a rotating island with a width of $\sim 25\%$ normalized by the plasma minor radius

is formed. In the second stage, in addition to the above-mentioned island, a non-rotating flattening with a width of 10% normalized by the plasma minor radius appears in the torus outboard side. In addition, the time evolution of the pressure degradation profile in the slowing-down phase was investigated. The pressure degradation region moves from slightly inside the resonant surface to the center of the plasma during the slowing-down phase.

Acknowledgments

The authors are grateful to the LHD experiment group for their excellent support. One of the authors (YT) would like to thank Dr. K. Ida, M. Goto, T. Morisaki, and Y. Suzuki for useful discussions. This work was supported in part by NIFS under contracts KLPH004, ULHH040, and UFEX105, and by JSPS KAKENHI (Nos. 15KK0245, 26709072, and 20K03910).

- [1] Y. Takemura *et al.*, Nucl. Fusion **52**, 102001 (2012).
- [2] S. Sakakibara *et al.*, Nucl. Fusion **55**, 083020 (2015).
- [3] S. Sakakibara *et al.*, Nucl. Fusion **53**, 043010 (2013).
- [4] M. Okamoto *et al.*, Nucl. Fusion **61**, 046005 (2021).
- [5] Y. Takemura *et al.*, Nucl. Fusion **59**, 066036 (2019).
- [6] Y. Takemura *et al.*, Plasma Fusion Res. **12**, 1402028 (2017).
- [7] T. Tokuzawa *et al.*, Nucl. Fusion **57**, 076003 (2017).
- [8] Y. Takemura *et al.*, Nucl. Fusion **61**, 026011 (2021).
- [9] I. Yamada *et al.*, Fusion Sci. Technol. **58**, 345 (2010).
- [10] K.Y. Watanabe *et al.*, Fusion Sci. Technol. **58**, 160 (2010).
- [11] T. Morisaki *et al.*, Fusion Sci. Technol. **58**, 465 (2010).
- [12] S. Sakakibara and H. Yamada, Fusion Sci. Technol. **1055**, 471 (2010).
- [13] H. Johnsen *et al.*, Phys. Fluids **30**, 2239 (1987).